Check for updates

Molybdenum disulfide composite materials with encapsulated copper nanoparticles as hydrogen evolution catalysts

Chuangye Wang, [ID]* Wenjing Zhao, Huixin Jiang, Mengyu Cui, Yu Jin, Ruixue Sun, Xufeng Lin [ID] and Longli Zhang*

In the current work, a series of molybdenum disulfide composite MCNTs@Cu@MoS$_2$ materials with high hydrogen evolution performance are prepared. In the hydrogen evolution reaction, their overpotential is as low as 225 mV at a current density of 10 mA cm^{-2} in 1 M H$_2$SO$_4$ as electrolyte solution. This excellent catalytic activity has been ascribed to its lower electrical impedance and high double layer capacitance. The encapsulation of copper nanoparticles into MoS$_2$ crystals significantly reduces their resistance, enhancing the electron transfer rate during water electrolysis. Thereby, the introduction of conductive nanoparticles into semi-conductive catalyst crystals would be an efficient measure to improve their electrochemical catalytic activity in the hydrogen evolution reaction.

1. Introduction

In the face of excessive carbon emission, the international community has reached an agreement that renewable energy sources should be developed to replace conventional fossil fuels.[1–5] Unlike other renewables such as solar, wind and tidal wave power, H$_2$ can be directly used in combustion engines and fuel cells. More importantly, it can be stored and transported in chemical form. These properties make it the most promising substitution to fossil fuels. Due to this background, the manufacture of H$_2$ by water electrolysis has attracted more and more interest.

The green routines to obtain a source of hydrogen are mainly concerned with electrolysis[6–8] and photocatalysis.[9,10] In both procedures, a catalyst with higher activity is crucial. As far as electrochemical hydrogen evolution is concerned, in the past decades, there have been a lot of publications reporting compound catalysts as alternative to the noble metals. Among these compounds, molybdenum disulfide was one of the most popular materials. Many of its derivatives have been intensively studied already. To improve the catalytic performance of those materials, some efficient strategies have been employed. One is to enlarge the specific number of active sites by, for example, exposing more edge sites by introducing more surface defects,[11–14] one is to dope either metallic or chalcogen heteroatoms into the lattice of this basal 2D catalyst to achieve synergistic effect,[15,16] and the other is to reduce the resistance of material for the sake of

achievement of a high current density with a lower overpotential in water electrolysis.[17–20] In the last routine, graphene and nanotube might be the most popular choice for conductivity enhancement. Besides, some metallic nanoparticles having either low resistance or high catalytic activity were also chosen to modify the catalytic performance of molybdenum disulfide.

Owing to its sheet structure, molybdenum disulfide exhibits a high electrical resistance leading to a higher overpotential in electrolysis of water. The goal of the current report is to enhance the conductivity of molybdenum disulfide by inserting copper nanoparticles into molybdenum disulfide crystals. Briefly spoken, the copper nanoparticles were first anchored onto the multi-walled carbon nanotubes (MCNTs) by reduction reaction, then, molybdenum disulfide (MoS$_2$) was hydrothermally synthesized based on this substrate to prepare the final product MCNT@Cu@MoS$_2$ composite materials. The characterizations of their structures evidenced a successful encapsulation of nanoparticles by MoS$_2$ crystals, and the tests of their catalytic performance in electrolysis of water showed that those composites can work with a lower overpotential in hydrogen evolution reaction. The method presented here might provide a facile method to synthesize efficient electrochemical catalysts for hydrogen evolution.

2. Experimental

2.1 Preparation of catalysts

2.1.1 (a). MCNTs@Cu@MoS$_2$. A typical preparation procedure is as follows. 1 g multi-walled carbon nanotubes (MCNTs, Xianfeng Nano) was fluxed by 150 mL mixture of H$_2$SO$_4$ (98%, Sinopharm) and HNO$_3$ (68%, Sinopharm) at 100 °C for 8 hours.

School of Chemistry & Chemical Engineering, China University of Petroleum (East China), Changjianxi Rd 66, 266580 Qingdao, China. E-mail: chwang@upc.edu.cn; zhangll@upc.edu.cn; Fax: +86-532-86981130; Tel: +86-532-86983361

After filtration, these acidized MCNTs were alternatively washed by distilled water and absolute alcohol (AR, Fuyu chemical in Tianjin) until pH reaching 7, and then dried in vacuum at 65 °C for another 8 hours.

0.1 g pretreated MCNTs was dispersed into 40 mL distilled water at room temperature. 0.0201 g $CuSO_4 \cdot 5H_2O$ (98%, Energy Chemical Shanghai), 3.2 mg polyvinyl pyrrolione K-30 (92%, Sinopharm) and 4.8 mg ethylenediamine tetraacetate (99.5%, Sinopharm) was in turn added into this dispersion at 60 °C with a stir. After the addition of hydrazine hydrate (85%, Sinopharm) and ammonia (25%, Sanhe Chemicals in Yantai) drop by drop, the reduced copper nanoparticles were generated. After filtration and drying in vacuum for 8 hours at 60 °C, the modified MCNTs with anchored nanoparticles were obtained and named as 1-MCNTs@Cu. Individually modulating the added amount of $CuSO_4 \cdot 5H_2O$ to 0.0402, 0.0804, 0.1206 and 0.1608 g and ethylenediamine tetraacetate to 9.6, 19.3, 28.9 and 38.6 mg, another four MCNTs@Cu samples with different copper contents were simultaneously prepared. They were separately named as 2-MCNTs@Cu, 3-MCNTs@Cu, 4-MCNTs@Cu and 5-MCNTs@Cu.

In the next stage, 0.1 g MCNTs@Cu was firstly dispersed into 50 mL aqueous solution of 1.33 g thiourea (98%, energy chemicals) by ultrasonic, then 0.6179 g $(NH_4)_2MoO_4$ (99.99%, energy chemicals) was added. The mixture was transformed into a Teflon-lined stainlesssteel autoclave to conduct hydrothermal crystallization at 190 °C for 48 hours. After naturally cooling to room temperature, black precipitates were collected by centrifugation. Those powders were dried at 80 °C for 8 hours after washed alternatively by distilled water and absolute ethanol for three times. The ultimate product was named as MCNTs@Cu@MoS$_2$. Following the name of MCNTs@Cu substrates, these prepared composite materials were separately labelled as 1-MCNTs@Cu@MoS$_2$, 2-MCNTs@Cu@MoS$_2$, 3-MCNTs@Cu@MoS$_2$, 4-MCNTs@Cu@MoS$_2$ and 5-MCNTs@Cu@ MoS$_2$.

2.1.2 (b). MCNTs@MoS$_2$. To shed light on the influences of encapsulated nanoparticles on both structure and catalytic performance in hydrogen evolution of those composites, the material MCNTs@MoS$_2$ without copper nanoparticles

encapsulated was synthesized simultaneously. Its preparation procedure was almost the same as described above, but no copper source was involved.

2.2 Structure

The crystal structures of the as-prepared materials were identified by powder X-ray diffraction (Shimadu, XRD-6000). Their surface morphology and specific surface area were separately characterized by scanning electron microscope (JEOL, JSM-7500F) and N$_2$ adsorption/desorption (Micromeritics, TriStar 3000). High resolution transmission electron microscope (FEI, Tecnai-G20) was also employed to give a more detailed insight into their crystal structures. Additionally, the elemental distribution within those samples were achieved by EDS elemental mapping (FEI, SuperX).

2.3 Electrochemical measurements

The electrochemical tests of prepared samples were conducted on a CHI660D electrochemical workstation with a three-electrode system incorporating a glass carbon electrode (GCE, 5 mm diameter), a saturated calomel electrode (SCE) as reference and a Pt as counter electrode. 0.5 M H$_2$SO$_4$ solution was used as electrolyte solution. The solution was bubbled with nitrogen to eliminate the dissolved oxygen before launching the test.

To fabricate the working electrode, the GCE was first polished for several times with 200 mesh aluminum oxide powders and then treated with the finer with 1 μm diameter. This GCE was then cleaned successively by 10% HNO$_3$, absolute ethanol and distilled water in ultrasonic bath before dried up in the air. 10 μL dispersion prepared with 4 mg catalyst powders and 1 mL ethanol solution of 0.1 mL Nafion (5% wt, Sigma-Aldrich) was dropped onto this GCE. Until the solvent evaporated at room temperature, the cathode for test got ready.

HER activities of all electrocatalysts were firstly assessed by linear sweep voltammetry with a speed of 1 mV s^{-1}. Cycling voltammetry (CV) was conducted separately with 40, 80, 120, 160 and 200 mV s^{-1} sweeping speeds to determine the electrochemical capacitance of catalysts. Electrochemical
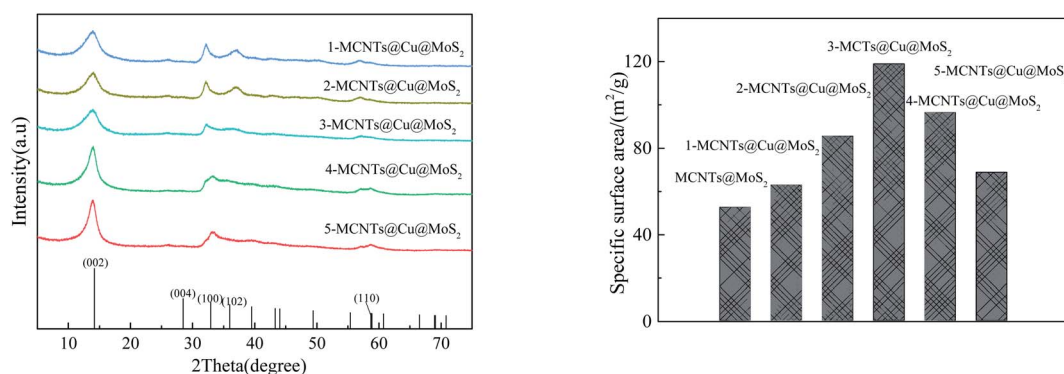

Fig. 1 XRD patterns and specific surface areas of prepared MCNTs@Cu@MoS$_2$ samples. The characteristic peaks exhibit the composite MoS$_2$ materials with a high relative crystallinity, and the sample 3-MCNTs@Cu@ MoS$_2$ has the highest specific surface area around 120 m^2 g^{-1}.
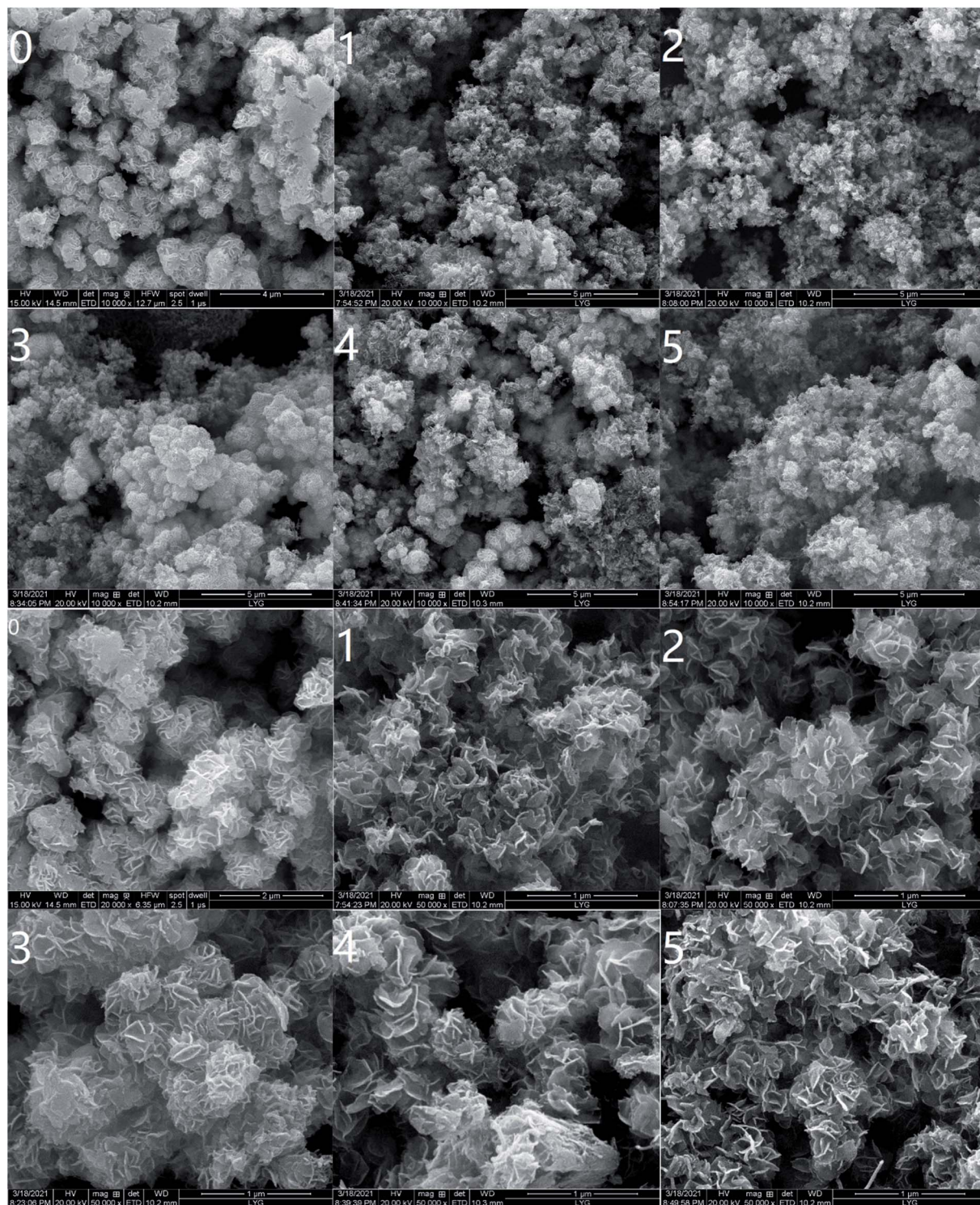
Fig. 2 SEM images of prepared MCNTs@MoS$_2$ (0) and MCNTs@Cu@MoS$_2$ samples (1–5) with two different magnifications.

impedance spectra (EIS) were obtained within a frequency range of 0.1–100 kHz with an overpotential of 400 mV. All potentials involved have been referenced to reversible hydrogen electrode according to $E(vs.\ \mathrm{RHE}) = E(vs.\ \mathrm{SCE}) + 0.2415 + 0.059$ pH.

3. Results and discussion

The XRD patterns in Fig. 1 demonstrate that all of the samples have characteristic peaks of MoS$_2$, indicating a high relative crystallinity. However, no signals from Cu crystal could be
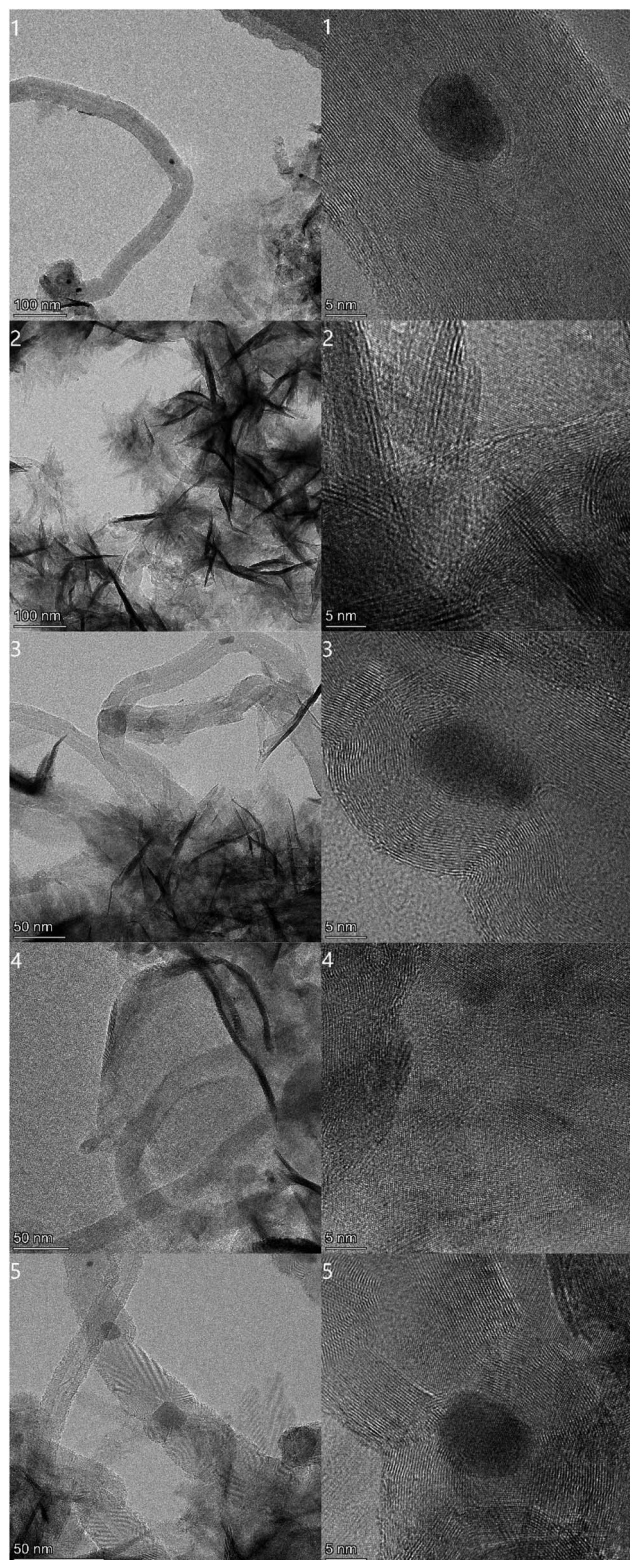
Fig. 3   TEM images of MCNTs@Cu@MoS$_2$ composites. The encapsulation of copper nanoparticles in MoS$_2$ crystal sheets is clearly evidenced.

Cu precursor used in the preparation procedure. On the other hand, those formed nanoparticles are encapsulated by MoS$_2$, not able to be sensitively detected. Nevertheless, the interlayer distances of (002), (100) and (110) planes separately indicated by 2theta = 14.2°, 33.1°, and 56.7° are extended by the increasing Cu content, manifesting that Cu particles are not simply mixed with MoS$_2$ crystals but encapsulated by them. The specific surface areas determined from N$_2$ adsorption/desorption isotherms are displayed in Fig. 1. All of five MCNTs@Cu@MoS$_2$ samples show higher specific surface areas than MCNTs@MoS$_2$, and 3-MCNTs@Cu@MoS$_2$ has the maximum value approximating to 120 m^2 g^{-1}.

Those SEM images have been compiled in Fig. 2, from which the morphology of prepared samples can be seen clearly. It is quite observant that the composite materials appear flower-like and are anchored on MCNTs@Cu substrate. This blooming-flower-like structure leads to a large specific surface area and provides much long edges, exposing numerous active sites to the interface between electrode and solution in electrolysis procedure. This characteristic is much favorable for an efficient hydrogen evolution process.

For a deep insight to the structure of the materials, TEM were employed. From the images displayed in Fig. 3, the encapsulation of Cu nanoparticles by MoS$_2$ can be observed. In the left column with a lower magnification, the metallic particles together with MoS$_2$ crystals are anchored on nanotubes. This feature will cause a higher electron conductivity of these samples when they work as catalyst to electrolyze water. In right column with higher magnification, the morphology of nanoparticles can be found clearly as dark dots. The insertion of Cu nanoparticles into MoS$_2$ crystals could profoundly improve the conductivity of those synthesized semi-conductive catalysts, enabling them to work with a higher current in electrolysis of water. The elemental distributions of those five as-prepared MCNTs@Cu@MoS$_2$ composites have been provided by EDS mapping for a further witness of the copper particles. They were displayed in Fig. 4. Those metallic particles have a very even distribution and do not agglomerate to form large blocks, demonstrating that the presented method is efficient and effective to introduce metallic nanoparticles into MoS$_2$ catalysts. Thereby, this technique could be useful to insert metallic particles during composite electrocatalyst preparation.

To unveil the advantages of the introduction of metallic particles, a series of electrochemical measurements have been conducted to evaluate their catalytic performances, as well as their own properties. The polarization curves are displayed in Fig. 5, together with corresponding Tafel slopes. Comparably, those composite catalysts with encapsulated nanoparticles reveal lower overpotentials at given currents, compared to MCNTs@MoS$_2$. According to those plots, all HERs these composites involved occur on Volmer–Heyrovsky mechanism. In the between, the Tafel slope of 3-MCNTs@Cu@MoS$_2$ is 81 mV Dec^{-1}, indicating a highest catalytic activity. This value is lower than 118 mV Dec^{-1} achieved by nitrogen doped hierarchical CoS$_2$/MoS$_2$[21] but approaches to that of hierarchical MoSe$_2$–CoSe$_2$.[22] Another reference metric able to indicate

found (though, their presence will be confirmed in the following sections). That is, on one hand, attributed to the low nanoparticle concentration resulting from the small amount of
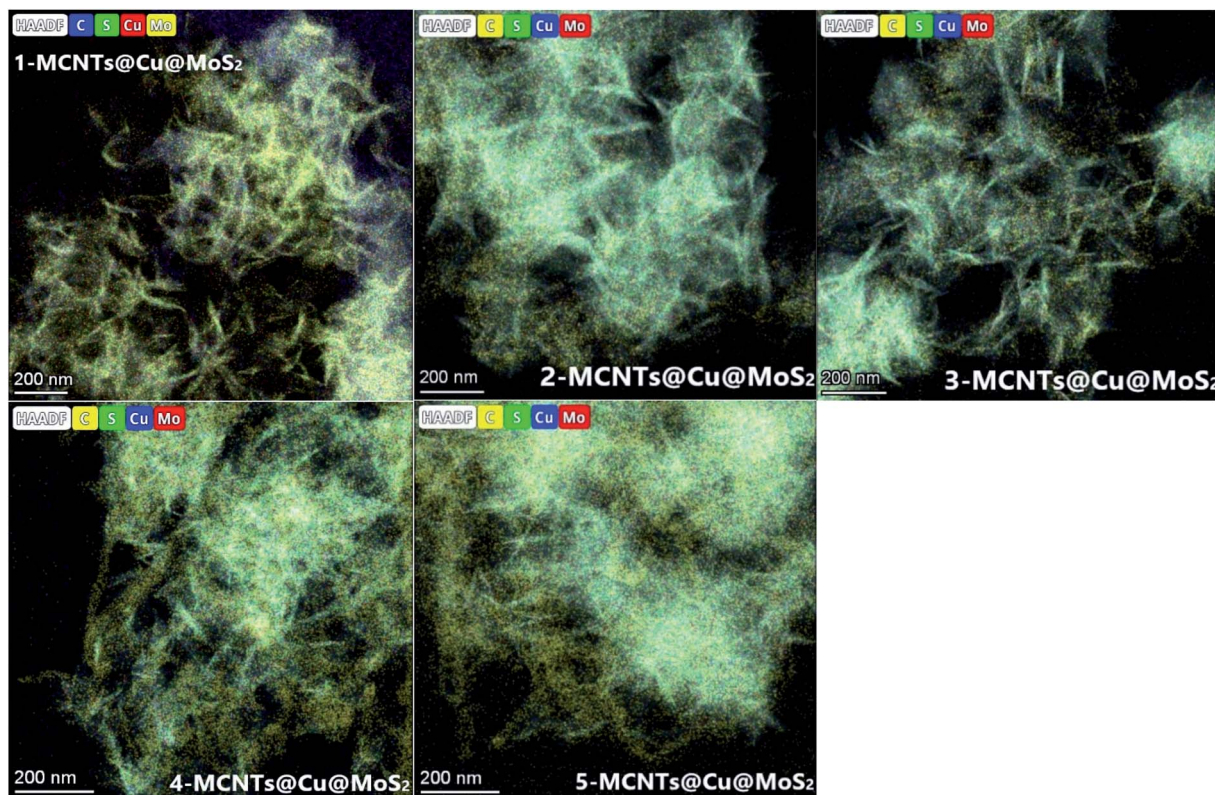
Fig. 4 Images of EDS elemental mapping. It can be noted that copper has an even distribution inside of the prepared materials.

catalytic performance is the overpotential value for current density 10 mA cm^{-2}. Concerning 3-MCNTs@Cu@MoS$_2$, it reads 225 mV, comparably higher than 184 mV achieved by similar material with optimal recipe,[7] and that of P[23] N,[24] Pt,[25] Pd[26] doped MoS$_2$, but still better than Co doped MoS$_2$.[25,27] Taking into account the Tafel slope, this 3-MCNTs@Cu@MoS$_2$ material showed a significant improvement compared to bare 2H phase MoS$_2$ nanosheets,[28] demonstrating that the incorporation of Cu nanoparticles can improve the charge communication for semi-conductive MoS$_2$ materials.

One of the most important measures of electrochemical active area is the double layer capacitance (C_{dl}). The C_{dl}s of all prepared samples retrieved from correspondent CV curves are plotted as Fig. 6. The introduction of Cu nanoparticle enhances the C_{dl} of MoS$_2$ from 10.50 to 21.69 mF cm^{-2}. The value of 21.69 mF cm^{-2} belongs to 3-MCNTs@Cu@MoS$_2$, evidencing that appropriate content of Cu nanoparticles can lead to a high double layer capacitance which facilitates to promote the hydrogen evolution reaction rate. The Nyquist plots obtained from electrochemical impedance spectroscopy conducted at
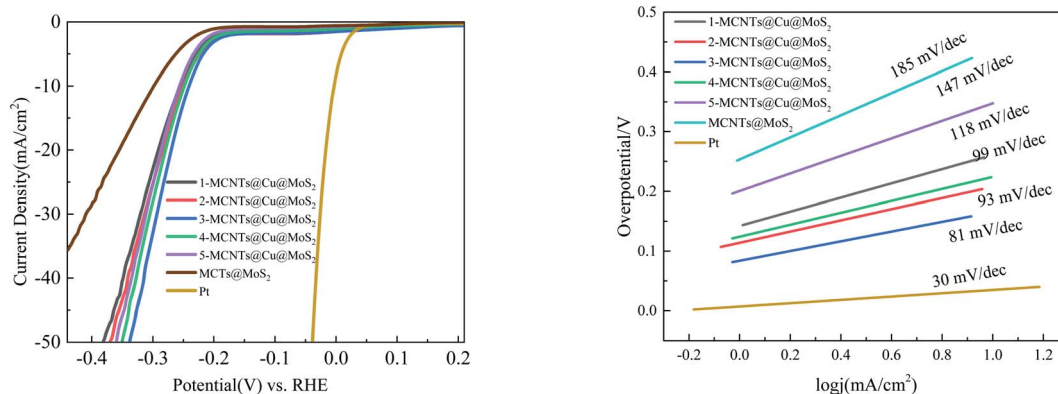

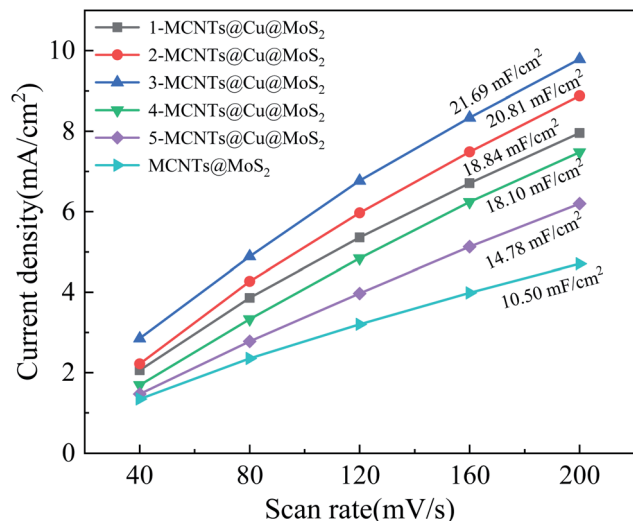**Fig. 5** Polarization curves and Tafel plots of as-prepared six samples.

Fig. 6 Double layer capacitance of the six samples. 3-MCNTS@Cu@MoS$_2$ possesses the highest double layer capacitance.

Fig. 8 Durability test for 3-MCNTs@Cu@MoS$_2$ in 0.5 M H$_2$SO$_4$ solution.

400 mV overpotential have been showed in Fig. 7, together with correspondent ohmic series resistance (R_s) and charge transfer resistance (R_{ct}). One can learn that all copper composites have lower charge transfer resistances than the sample MCNTs@MoS$_2$ without copper. Thereinto, 3-MCNTs@Cu@MoS$_2$ has the lowest ohmic series resistance (R_s) and charge transfer resistance (R_{ct}), namely 148.6 and 9.4 Ω, respectively. Those are significantly reduced separately from 354 and 22.2 Ω of the sample MCNTs@MoS$_2$. The above results demonstrate that the introduction of Cu nanoparticles has profoundly modified double layer capacitance and resistances of bare MCNTs@MoS$_2$, and thus, enhanced the catalytic performances of composites by speeding the electron transfer rate, as HER tests showed. The durability of 3-MCNTs@Cu@MoS$_2$ electrode in catalytic reaction was also tested. Linear scanning voltage was employed for 1000 and 10 000 circles. The curves in Fig. 8 show that within 1000 circles significant degradation can hardly be found, and after 10 000
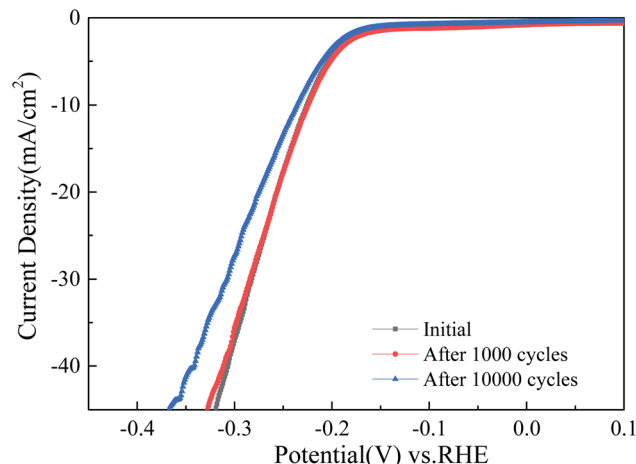
circles the overpotential shifts to 236 mV from initial 225 mV with 10 mA cm^{-2} current density. Generally, a good structural stability can be evidenced. The dissolution of Cu in the electrolyte solution is not observed within this test period. All of above electrochemical properties can consistently illustrate the reason why the sample 3-MCNTs@Cu@MoS$_2$ possesses the most excellent catalytic performance in HER. According to XPS spectra in Fig. 9, the molar ratio of copper to molybdenum disulfide in sample 3-MCNTs@Cu@MoS$_2$ has also been determined by peak intensities of Cu p$_{3/2}$ and Mo d$_{5/2}$ core levels taking into account their photoionization cross sections. The amount of copper is around 4 percent of molybdenum disulfide. That the encapsulation of such a low amount of conductive metallic nanoparticles leads to such a significant improvement of electrocatalytic performance demonstrates that the insertion of metallic particles can indeed efficiently improve the catalytic behavior of molybdenum disulfide. Lower resistance, higher surface active area and higher double layer capacitance facilitate to speed the electron transfer rate, and thus, to accelerate
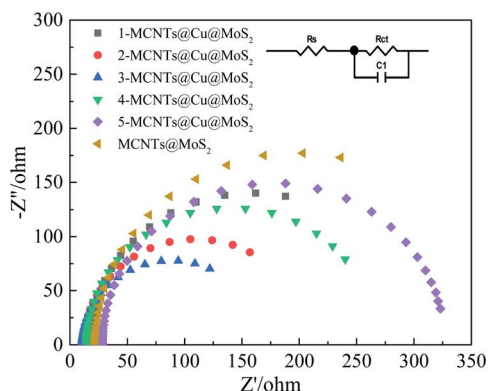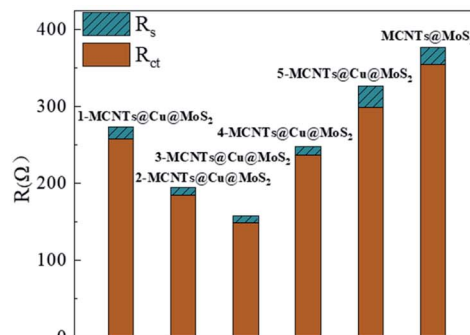

Fig. 7 Nyquist plots with correspondent ohmic series resistance (R_s) and charge transfer resistance (R_{ct}) of all prepared materials.
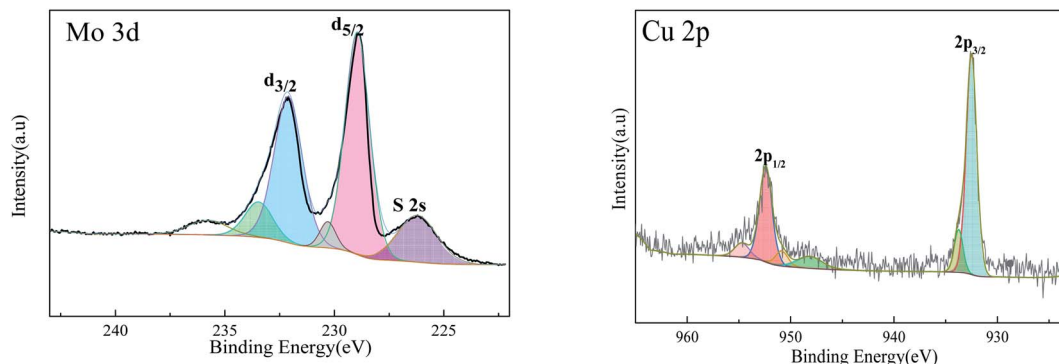
Fig. 9 XPS spectra of Mo 3d and Cu 2p core levels. The intensity of peaks is used to determine the stoichiometric relationship of species.

the electrolysis rate. Thereby, the strategy introducing copper nanoparticle into the catalyst crystals is successful.

4.   Summary and conclusions

In the present work, MoS_2 composites with encapsulated copper nanoparticles on multi-walled carbon nanotubes are hydrothermally synthesized with general chemicals. The results show that the material 3-MCNTs@Cu@MoS_2 with optimal recipe exhibits a superior catalytic performance in electrolysis of water to obtain hydrogen. It can work at a lower overpotential with a high current. The causes leading to those excellent behaviors are owed to its low impedance, higher double layer capacitance and higher surface area which benefit further from the encapsulation of copper nanoparticles.

People have dispersed metallic particles onto the surfaces of prepared MoS_2 materials. Some of those particles, for example platinum, worked as co-catalyst and a high efficiency in water electrolysis have been achieved. The goal of the present work is simply through introducing highly conductive metallic particles into semi-conductive MoS_2 material to significantly enhance their conductivity and improve their electrochemically catalytic performance. The results presented here have turned out that this strategy is reliable and fulfilling to prepare similar electrochemical catalysts with lower overpotentials in electrolytic reactions.

Conflicts of interest

The authors have no competing interest to declare.

Acknowledgements

References

1 A. J. Turner, *Science*, 1999, **285**, 687–689.

2 N. Z. Muradov and T. N. Veziroglu, *Int. J. Hydrogen Energy*, 2008, **33**, 6804–6839.

3 X. Zou and Y. Zhang, *Chem. Soc. Rev.*, 2015, **44**, 5148–5180.

4 M. Goetz, J. Lefebvre, F. Moers, A. M. Koch, F. Graf, S. Bajohr, R. Reimer and T. Kolb, *Renewable Energy*, 2016, **85**, 1371–1390.

5 B. Pivovar, N. Rustagi and S. Satyapal, *Electrochem. Soc. Interface*, 2018, **27**, 47–52.

6 A. Li, H. Ooka, N. Bonnet, M. T. Hayashi, Y. Sun, Q. Jiang, C. Li, H. Han and R. Nakamura, *Angew. Chem., Int. Ed.*, 2019, **58**, 5054–5058.

7 M. Carmo, D. L. Fritz, J. Mergel and D. Stolten, *Int. J. Hydrogen Energy*, 2013, **38**, 4901–4934.

8 K. Fujii, S. Nakamura, M. Sugiyama, K. Watanabe, B. Bagheri and Y. Nakano, *Int. J. Hydrogen Energy*, 2013, **38**, 14424–14432.

9 A. Fujishima and K. Honda, *Nature*, 1972, **238**, 32–37.

10 D. Kang, T. Kim, S. Kubota, A. Cardiel, H. Cha and K. Choi, *Chem. Rev.*, 2015, **115**, 12839–12887.

11 D. Kong, H. Wang, J. Cha, M. Pasta, K. Koski, J. Yao and Y. Cui, *Nano Lett.*, 2013, **13**, 1341–1347.

12 Y. Zhang, Q. Ji, G. Han, J. Ju, J. Shi, D. Ma, J. Sun, Y. Zhang, M. Li, X. Lang, Y. Zhang and Z. Liu ZF, *ACS Nano*, 2014, **8**, 8617–8624.

13 M. R. Islam, N. Kang, U. Bhanu, H. P. Paudel, M. Erementchouk, L. Tetard, M. N. Leuenberger and S. I. Khondaker, *Nanoscale*, 2014, **6**, 10033–10039.

14 B. Qiao, A. Wang, X. Yang, L. F. Allard, Z. Jiang, Y. Cui, J. Liu, J. Li and T. Zhang, *Nat. Chem.*, 2011, **3**, 634–641.

15 G. Vile, D. Albani, M. Nachtegaal, Z. Chen, D. Dontsova, D. Antonietti, N. Lopez and J. Perez-Ramirez, *Angew. Chem., Int. Ed.*, 2015, **54**, 11265–11269.

16 F. Z. Yan, C. K. Liao, G. H. Wu, S. B. Bach and M. A. Mahmoud, *J. Phys. Chem. C*, 2019, **123**, 29856–29865.

17 F. Li, J. Li, X. Lin, X. Li, Y. Fang, L. Jiao, X. An, Y. Fu, J. Jin and R. Li, *J. Power Sources*, 2015, **300301–300308**.

18 D. Li, U. N. Maiti, J. Lim, D. S. Choi, W. J. Lee, Y. Oh, G. Y. Lee and S. O. Kim, *Nano Lett.*, 2014, **14**, 1228–1233.

19 A. B. Laursen, P. Vesborg and I. Chorkendorff, *Chem. Commun.*, 2013, **49**, 4965–4967.

20 B. N. Darshan, A. Kareem, T. Maiyalagan and V. E. Geo, *Int. J. Hydrogen Energy*, 2021, **46**, 13952–13959.

21 X. Wang, B. Zheng, B. Wang, H. Wang, B. Sun, J. He, W. Zhang and Y. Chen, *Electrochim. Acta*, 2019, **299**, 197–205.

22 H. Vrubel, T. Moehl, M. Graetzel and X. Hu, *Chem. Commun.*, 2013, **49**, 8985–8987.

23 R. Li, L. Yang, T. Xiong, Y. Wu, L. Cao, D. Yuan and W. Zhou, *J. Power Sources*, 2017, **356**, 133–139.

24 M. Acerce, D. Voiry and M. Chhowalla, *Nat. Nanotechnol.*, 2015, **10**, 313–318.

25 J. Deng, H. Li, J. Xiao, Y. Tu, D. Deng, H. Yang, H. Tian, J. Li, P. Ren and X. Bao, *Energy Environ. Sci.*, 2015, **8**, 1594–1601.

26 Z. Luo, Y. Ouyang, H. Zhang, M. Xiao, J. Ge, Z. Jiang, J. Wang, D. Tang, X. Cao, C. Liu and W. Xing, *Nat. Commun.*, 2018, **9**, 1–8.

27 T. H. M. Lau, X. Lu, J. Kulhavy, S. Wu, L. Lu, T. S. Wu, R. Kato, J. S. Foord, Y. L. Soo, K. Suenaga and S. C. E. Tsang, *Chem. Sci.*, 2018, **9**, 4769–4776.

28 D. Voiry, M. Salehi, R. Silva, T. Fujita, M. Chen, T. Asefa, V. B. Shenoy, G. Eda and M. Chhowalla, *Nano Lett.*, 2013, **13**, 6222–6227.